Available online at www.sciencedirect.com
ScienceDirect
Journal of the European Ceramic Society 31 (2011) 2129–2135
www.elsevier.com/locate/jeurceramsoc

# Synthesis of α-SiC/α-SiAlON composites by spark plasma sintering: Phase formation and microstructures development

Limeng Liu *, Feng Ye, Xiulan He, Yu Zhou

*School of Materials Science and Engineering, Harbin Institute of Technology, Harbin 150001, China*

Received 5 February 2011; received in revised form 2 May 2011; accepted 15 May 2011
Available online 8 June 2011

**Abstract**

α-SiC/α-SiAlON composites with 80 wt% α-SiC (6H phase) were fabricated by spark plasma sintering at 1800–2000 °C in a 0.6 atm nitrogen atmosphere. The effects of the temperatures on the phase development, microstructures and mechanical properties were investigated. The results showed the $Si_3N_4$, AlN, $Al_2O_3$, and $Y_2O_3$ particles were isolated by the 6H-SiC to prevent α-SiAlON formation at 1800 °C. The $Si_3N_4$ decomposed at 1900 °C and above, thus added Si in the phase compositions. The α-SiC grains grew anisotropic in the sintering liquids at 1800 °C and 1900 °C, forming the self-reinforcing microstructures, and accordingly increased the flexural strength and fracture toughness. In cooling down immediately after the temperature reached 2000 °C, a transitory hold at 1700 °C transformed the 6H-SiC into the 3C polytype in 30 s. The electric current was suspected of activating this polytype transformation.


*Keywords:* Carbide; A. Sintering; Microstructure; C. Strength; E. Structural applications

## 1. Introduction

Silicon carbide ceramics are a common commercial structural material. They can be used at high-temperatures up to 1300 °C due to high chemical stability, oxidation resistance, good thermal shock resistance and creep resistance [1–4].

Generally, SiC ceramics are very difficult to densify and have relatively low fracture toughness. These problems are usually dealed with by the liquid sintering techniques, using $Al_2O_3$, $Al_2O_3$–$Y_2O_3$, or Al-B-C as the sintering adds [5–11]. The oxides react with the $SiO_2$ present on the surfaces of the SiC particles to form the liquid phases that promote densification. α-SiC grains grew anisotropic to form the desired self-reinforcing microstructures. Fracture toughness can be increased by folds, from 2–4 MPa $m^{1/2}$ to 6–9 MPa $m^{1/2}$.

However, the sintering liquids always result in an obvious disadvantage. Upon cooling, the liquids either partly crystallize or remain completely glassy [6,9,10]. As a result, the high-temperature properties such as creep and oxidation resistance of the materials [1–4] are deteriorated. Annealing and using more refractory additives are tried but not satisfactory. On the other hand, solubilities of the $Al^{3+}$, $Y^{3+}$, $O^{2-}$, and $N^{3-}$, etc. in the SiC lattice are very limited [7], making incorporation of the liquid ingredients into the crystal lattices infeasible.

The α-SiAlON/SiC composites seem to be a better choice for the solid solution nature of the α-SiAlON phase. α-SiAlON is a solution of the α-$Si_3N_4$ with a general formula of $RE_{m/v}Si1_{2-(m+n)}Al_{m+n}O_nN_{16-n}$ ($RE^{v+}$ = $Li^+$, $Ca^{2+}$, $Y^{3+}$, $Yb^{3+}$, $Dy^{3+}$, $Nd^{3+}$, etc., and $1.0 < m, n < 2.5$) [12–17]. During SiAlON formation, the AlN, $Al_2O_3$, and the RE oxides particles in the starting materials react with the $SiO_2$ on the $Si_3N_4$ surfaces to produce a remarkable concentration of transient liquid. After densification, most of the $RE^{v+}$, $Al^{3+}$, $O^{2-}$, $N^{3-}$ species are incorporated into the α-SiAlON lattice, and sharply reduces the contents of the intergranular phases. Clearly, this liquid elimination effect can also be expected in the α-SiAlON/SiC system. In addition, because of the appearance of the sintering liquids, α-SiAlON and SiC can grow anisotropic. Therefore, a self-reinforcing microstructure is expectable.

A few literatures have tried the SiAlON/SiC composites by hot isostatic pressing (HIP), hot pressing (HP) and gas pressure sintering (GPS) [18–22]. However, the desired self-toughening microstructures were not obtained. Neither the SiAlON nor the SiC grains grew anisotropic.

* Corresponding author. Tel.: +86 451 86413921; fax: +86 451 86413921.
*E-mail addresses:* liulimeng@hit.edu.cn, llm6812@yahoo.com.cn (L. Liu).

0955-2219/$ – see front matter © 2011 Elsevier Ltd. All rights reserved.
doi:10.1016/j.jeurceramsoc.2011.05.013

Our previous study demonstrated that the self-toughening microstructures could be developed by spark plasma sintering (SPS) [23]. In this work, the effects of the SPS temperatures on the phase compositions, microstructures and mechanical properties of the α-SiAlON/SiC composites with 20 wt% α-SiAlON were detailed. The influences of passing a high electric current through the densified SiAlON/SiC compact on the 6H → 3C-SiC phase transformation were also concerned, inspired by the observations that electric current can accelerate phase transformation in metals.

## 2. Experimental

The starting compositions of the investigated α-SiAlON/α-SiC composites are listed in Table 1. 20 wt% α-SiAlON was added to the α-SiC. The composition of the α-SiAlON phase was $Y_{1/3}Si_{10}Al_2ON_{15}$, i.e. $m$, $n = 1.0$ in the general formula $RE_{m/3}Si_{12-(m+n)}Al_{m+n}O_n\ N_{16-n}$ for α-SiAlON. 4 wt% $Y_2O_3$ was used as the sintering aid.

The starting materials were the commercial α-SiC (dominant 6H polymorph with ~6.7% 15R. Saint-Gobain Abrasives, Shanghai, China), $Si_3N_4$ (Grade E10, UBE Industries Ltd., Tokyo, Japan), $Al_2O_3$ (Grade A16SG, Alcoa, USA), AlN (grade C, H.C. Stark, Berlin, Germany) and $Y_2O_3$ (grade C, H.C. Stark, Berlin, Germany). Technical characters of the powders are listed in Table 1. The powder mixture was mixed in a plastic bottle using absolute alcohol and zirconia balls as the mixing media. The slurry was dried at 80 °C in a rotary evaporator and then passed through a 100 mesh screen.

A batch of 5 g of the powder mixture was loaded in a 40 mm-height SPS die with outer and inner diameter of 50 mm and 20 mm respectively. The die was lined by a 0.2 mm-thick graphite sheet for easy extrusion of the sintered compact. The SPS equipment was a Dr. Sinter 1080 (Sumitomo Coal Mining Co. Ltd., Tokyo, Japan). The sintering temperatures were monitored by a pyrometer focusing on the outer surface of the die.

After being evacuated, the SPS chamber was backfilled with nitrogen to 0.5 atm. At the temperature range of 1800–2000 °C, the gas pressure could reach 0.6 atm, mainly due to heating by the irradiation. Four sintering schedules were used. For all the schedules, the temperature was increased automatically to 700 °C in 4 min, the pressure simultaneously increased from 5 MPa to 30 MPa at the first stage. Then in schedule 1 and schedule 2, a heating rate of 100 °C/min was used to reach the preset 1800 °C or 1900 °C, respectively. After hold for 5 min, the pressure was released and SPS power was shut off.

For the third schedule, the temperature was increased from 700 °C to 1700 °C at 100 °C/min, further to 2000 °C at 300 °C/min (2029 °C was reached due to over heating), and followed by immediate shut off the SPS power. Average cooling rate of 360 °C/min from the max 2029 °C to 1700 °C was observed. For schedule 4, a short period of SPS heating was added immediately when the temperature was cooled to 1700 °C. For this transitory heating, a max power output up to 14.5 kW (voltage value of 6.2 V and current of 2332 A) was manually performed and accordingly lingered the temperature at 1700 °C for about 30 s, and then shut off the SPS power.

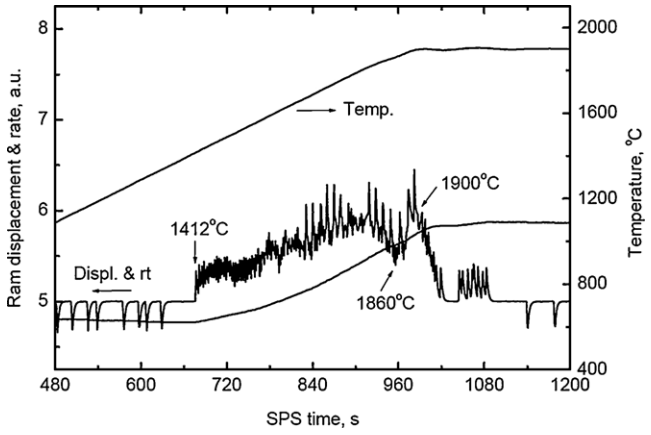


Fig. 1. SPS ram displacement as a function of temperatures, showing densification process of the α-SiC/α-SiAlON composite. $Si_3N_4$ decomposed at 1900 °C.

Schedule 3 and schedule 4 were arranged in order to compare the effects of passing the SPS electric current through the densified compact on the phases and microstructures of the materials.

All the as-sintered materials were designated by both the sintering temperatures and the dwelling times (Table 2). For instance, the 2000 °C 0 min + 1700 °C 0.5 min material was the composite fabricated by SPS at 2000 °C for 0 min and plus hold for 30 s at 1700 °C in the cooling down process (i.e. schedule 4).

The sintered samples were ground to eliminate possible contamination from the graphite die, then sliced, and polished to 0.5 μm diamond finish. Densities were measured by the Archimedes' principle. Phase compositions were investigated by X-ray diffraction (XRD) using Cu Kα irradiation. Vickers hardness was measured under 49 N load and dwell for 15 s. Flexure strength and fracture toughness were measured by three-point bending and single-edge-notched beam method respectively. The dimensions of the three-point bending samples were 4.0 mm × 1.5 mm × 18.0 mm with a 15.0 mm span. The dimensions of the single-edge-notched beams were 4.0 mm × 1.5 mm × 18.0 mm using a 16.0 mm span. A 2.0 mm deep notch was cut by a 0.2 mm thick diamond saw. The tensile side of the specimens for the strength and toughness test was normal and parallel to the SPS pressing direction respectively. Three specimens were tested for each condition and standard errors were calculated. Microstructures and fracture surfaces were observed by scanning electron microscopy (SEM) with energy dispersive X-ray spectroscopy (EDXS).

## 3. Results

### 3.1. Densification process

The densification processes of the α-SiC/α-SiAlON composites were illustrated by Fig. 1. The SPS ram travels indicated that the densification was initiated and completed at 1412 °C and 1860 °C, respectively. The two additional shrinkages at 1900 °C were attributable to $Si_3N_4$ decomposition and Si loss by evaporation.

Table 1
The starting composition of the investigated materials and characterization of the various powders.

| Powder | Starting composition (wt%) | Manufacturer | Product type | Purity and principle impurities[a] (wt%) | Particle size,[b] $d_{50}$ (μm) |
|---|---|---|---|---|---|
| α-SiC | 80.000 | Saint-Gobain Abrasives | SIKA SINTEX 13C | SiC > 98.5; free C < 0.3; O < 1.8; Si < 0.5 | 1.0–1.2 |
| α-$Si_3N_4$ | 15.308 | UBE Industries Ltd. | Grade E10 | α-$Si_3N_4$ > 95; O < 2.0; C < 0.2; Fe < 0.01; Al, Ca < 0.005; Cl < 0.01 | 0.5 |
| $Al_2O_3$ | 0.094 | Alcoa | Grade A16SG | α-$Al_2O_3$ > 99.9; $SiO_2$ < 0.01; $Fe_2O_3$ < 0.01; NaO < 0.08 | 0.2–0.4 |
| AlN | 2.603 | H.C. Stark | Grade C | AlN > 96; Fe < 0.005; O < 2.0 | 0.8–1.8 |
| $Y_2O_3$ | 1.995 | H.C. Stark | Grade C | $Y_2O_3$/TREO > 99.95[c] | 0.9 |

[a] Inspection of the manufacturer.
[b] By laser diffraction.
[c] TREO = total rare earth oxides.

Table 2
Sintering conditions, density, phase composition and mechanical properties of the composites.

| Sintering conditions | Density (g/cm$^3$) | Crystalline phases | $H_{v10}$ (GPa) | $K_{IC}$ (MPa m$^{1/2}$) | $\sigma$ (MPa) |
|---|---|---|---|---|---|
| 1800 °C 5 min | 3.006 | 6H-SiC | 21.7 ± 0.9 | 3.9 ± 0.4 | 295 ± 27 |
| 1900 °C 5 min | 3.201 | 6H-SiC, Si | 20.9 ± 0.8 | 5.6 ± 0.6 | 473 ± 43 |
| 2000 °C 0 min | 3.106 | 6H-SiC, Si, $Y_2Si_3O_3N_4$ and $Si_3Al_{12}O_9N_{10}$ | 18.7 ± 0.7 | 3.7 ± 0.5 | 447 ± 47 |
| 2000 °C 0 min plus 1700 °C 0.5 min | 3.097 | 3C-SiC, Si | 19.1 ± 0.7 | 4.5 ± 0.4 | 329 ± 35 |

The Archimedes' measurements results are listed in Table 2. SPS at 1800–2000 °C produced dense α-SiC/SiAlON composites. No open porosities were detected by the density measurements. For details of the effects of the sintering temperatures on the densities, the 1800 °C 5 min material (refer to sintering schedule 1) had the lowest density of 3.01 g/cm$^3$, while the 1900 °C 5 min material (sintering schedule 2) showed the largest 3.20 g/cm$^3$. When the sintering temperatures were further increased to 2000 °C for sintering schedules 3 and 4, densities of the resultant materials decreased slightly to 3.11 g/cm$^3$ and further to 3.10 g/cm$^3$ in the 2000 °C 0 min and 2000 °C 0 min + 1700 °C 0.5 min material, respectively. The differences in density values could be associated with the phase compositions, which were temperature dependent. For example, the lower density for the 2000 °C 0 min material could be caused by some Si concentration in the microstructure.

### 3.2. Phase formation

The XRD patterns of the different materials are shown in Fig. 2. The crystalline phases identified are listed in Table 2. SiC dominated all the phase compositions. In the 1800 °C, 1900 °C 5 min and the 2000 °C 0 min materials, the SiC phase was the same 6H-SiC polytype as in the starting material, while the 6H-SiC transformed into 3C (β-SiC) as shown in Fig. 2 the XRD patterns of the 2000 °C 0 min + 1700 °C 0.5 min material.

No α-SiAlONs were detected in the different materials, though the α-SiAlON phase and the different SiC polytypes had good phase compatibilities [18–22]. The absence of the α-SiAlON in the 1800 °C 5 min material was presumably due to the high dispersion of the $Si_3N_4$, AlN, $Al_2O_3$ and $Y_2O_3$ particles in the powder mixture. The small concentrations of the oxides and nitrides were isolated by the SiC particles. The mass diffusion of the α-SiAlON ingredients in the short holding time of 5 min at the relatively low temperature of 1800 °C was insufficient for the α-SiAlON formation. α-SiAlON may precipitate by prolonging the holding. Another possible reason was the significant amount of $SiO_2$ on the SiC particles, because it was not taken into account when calculating the starting composition. The SiAlON composition could have been altered by the extra $SiO_2$.

The 0.6 atm nitrogen atmosphere seemed not enough to inhibit $Si_3N_4$ dissociation at temperatures above 1900 °C. Si phase was presented in the 1900 °C 5 min and 2000 °C 0 min materials, as shown by Fig. 2. A weight loss of about 7.75% in the 1900 °C material was noticed. Because this value was much larger than that for complete $Si_3N_4$ dissociation (~6.1%), Si evaporation probably happened. The $Si_3N_4$ decomposition and subsequent Si evaporation could have caused the additional SPS ram travels at 1900 °C in Fig. 1.

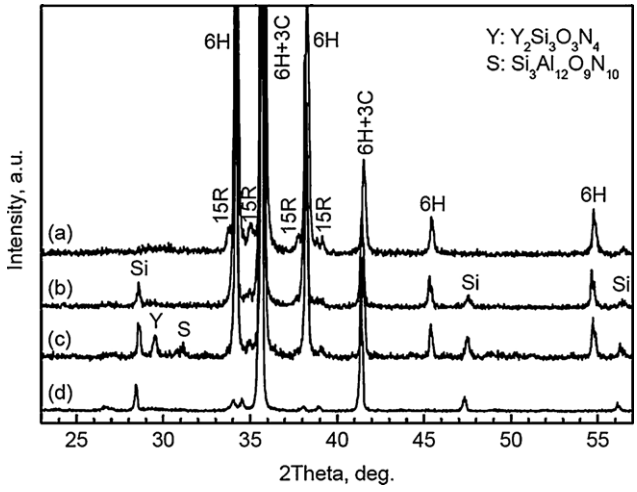


Fig. 2. XRD patterns of the materials synthesized under different SPS conditions, (a) 1800 °C, 5 min; (b) 1900 °C, 5 min; (c) 2000 °C, 0 min; and (d) 2000 °C, 0 min plus 1700 °C for 0.5 min.

The $Si_3N_4$ dissociation depleted the mayor α-SiAlON ingredient and accounted for the α-SiAlON absence in the phase compositions of the materials sintered at 1900 °C and above. Consequently, the $Al_2O_3$, AlN, $Y_2O_3$ were preserved and reacted with the $SiO_2$ on the SiC particles to form a "permanent" instead of the "transient" liquid that would be incorporated into the α-SiAlON lattices. Upon cooling the liquids crystallized as $Y_2Si_3O_3N_4$ and $Si_3Al_{12}O_9N_{10}$ in the 2000 °C 0 min material. However, the absent X-ray diffractions suggested their glassy natures of the solidified secondary phases in the other materials. The reason why the liquid showed different crystallization abilities in the different materials is intriguing but is not clear.

### 3.3. Microstructure development

The microstructures of the different materials are shown in Fig. 3. No residual pores were observed in the SEM micrographs, indicating full densities. For all the materials, the bright contrast was attributed to the YSiAlON phase, crystalline in the 2000 °C 0 min material but glassy in the others. The YSiAlON liquids wetted the SiC particles and infiltrated the grain boundaries. In the 2000 °C 0 min material, crystallization of the $Y_2Si_3O_3N_4$ and $Si_3Al_{12}O_9N_{10}$ phases depleted the intergranular YSiAlON, therefore the intergranular glassy phase was significantly reduced.

Dark areas in the microstructure of the 1800 °C 5 min material were mostly grain pulloff. The small grain sizes in the 1800 °C material made the grain boundaries prone to polishing fatigue. Due to lack of α-SiAlON formation, an Al–O–N rich phase was occasionally recognized in the 1800 °C 5 min material. This Al–O–N phase also had a dark contrast.

In the microstructures of the 1900 °C 5 min and 2000 °C 0 min materials in Fig. 3, the phases showed the darkest contrast were the Si product from the $Si_3N_4$ decomposition. The Si was distributed along with the gray SiC grains, indicating its preference of wetting the SiC particles.

Fig. 3 shows the SiC grains were elongated to have a mean diameter of 1.2 μm and aspect ratio up to 6 in the 1800 °C 5 min material. The grain elongation rather than the equiaxed morphology of the starting SiC particles was attributed to the Ostwald ripening happened in the sintering liquids. The projected parts of the irregular SiC particles should have dissolved in the surrounding liquids, then relocated and grew the elongated SiC grains. This grain growth behavior was different from the usual microstructure formation in the self-toughening SiC ceramics, where the microstructure was formed mainly by the 3C to 4H-SiC polytype transformation [6,7,10,11].

When the sintering temperatures were increased to 1900 °C and above, the 6H SiC grains grew slowly to 2.2 μm and 3.1 μm in average diameter in the 1900 °C 5 min and 2000 °C 0 min material, respectively. In comparison, fast grain growth happened in the 2000 °C 0 min + 1700 °C 0.5 min material. The average diameter of the 3C-SiC grains transformed from the 6H phase reached 15 μm (Fig. 3). Some YSiAlON was entrapped in the large 3C SiC grains suggesting the fast movement of the grain boundaries.

### 3.4. Mechanical properties

The mechanical properties of the different materials are listed in Table 2. The Vickers hardness, flexure strength, and fracture toughness in the range of ∼21.7 GPa, ∼473 MPa and ∼5.6 MPa $m^{1/2}$ respectively, were typical for a SiC ceramic [7]. The commercial SiC materials had flexure strength and fracture toughness of ∼400 MPa and ∼4 MPa $m^{1/2}$. The lower Vickers hardness than the reported 24 GPa was explainable by the large concentration of the intergranular YSiAlON and Si in the materials.

The largest Vickers hardness of 21.7 GPa observed in the 1800 °C 5 min material was due to the finer microstructure, similar to $Si_3N_4$ ceramics. $Si_3N_4$ ceramics having fine microstructure usually exhibited higher hardness than coarse microstructures [24]. Although the SiC grains showed the anisotropic growth, they were too small to perform significant load transfer and toughening mechanisms, hence relatively low flexure strength and fracture toughness for the 1800 °C 5 min material.

Maximum mechanical properties were reached in the 1900 °C 5 min material, with the best flexure strength and fracture toughness up to 473 MPa and 5.6 MPa $m^{1/2}$, respectively. The further elongated growth of the 6H SiC grains explained both the strength and the toughness improvements [25]. When the sintering temperature was further increased to 2000 °C, the flexure strength of the obtained 2000 °C 0 min material decreased slightly to 447 MPa, and the fracture toughness loss was more remarkable. Table 2 showed the 2000 °C 0 min material had the lowest toughness of 3.7 MPa $m^{1/2}$.

The fractographs of the different materials are shown in Fig. 4. Intergranular fractures dominated the fracture modes. Although the crack propagation along the grain boundaries which produced the intergranular fractures, was usually expected to result in high fracture toughness, the investigated materials only had moderate fracture toughness as shown in Table 2. The inferior mechanical properties than the reported values, may be explainable by the over-weakened interfacial bonding by the Si segregation along with the SiC grains, especially for the 2000 °C 0 min material as shown in Fig. 3. This Si segregation gave profound interfacial debonding as shown in Fig. 4. But the over-weakened interfacial bonding strength degraded both the strength and the toughness.

## 4. Discussion

### 4.1. Optimal sintering temperatures

The original aim of investigating the α-SiC/α-SiAlON composites was to synthesize a ceramic composite having elongated α-SiC grains in the microstructure. The ideal achievement would be that the transient liquid before α-SiAlON formation densified the composites. Then the α-SiC grains grew anisotropic in the transient liquid to improve mechanical properties. After densification and SiC grain growth, the $Y^{3+}$, $Al^{3+}$, $Si^{4+}$, $O^{2-}$, $N^{3-}$ species in the sintering liquid were incorporated into the α-SiAlON lattice. Therefore, the contents of the intergranular phases were reduced, benefiting the high high-temperature

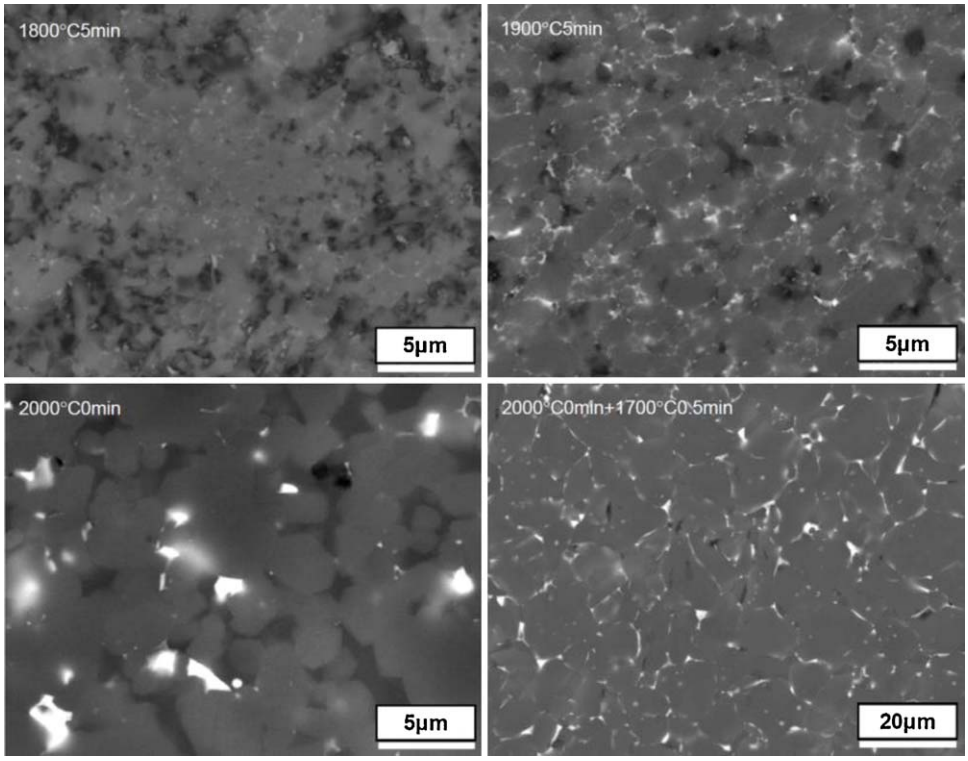


Fig. 3. SEM images of the microstructures for the investigated materials. 6H-SiC grains grow by Ostwald ripening, but transform into 3C phase in 0.5 min at 1700 °C during cooling down from 2000 °C.

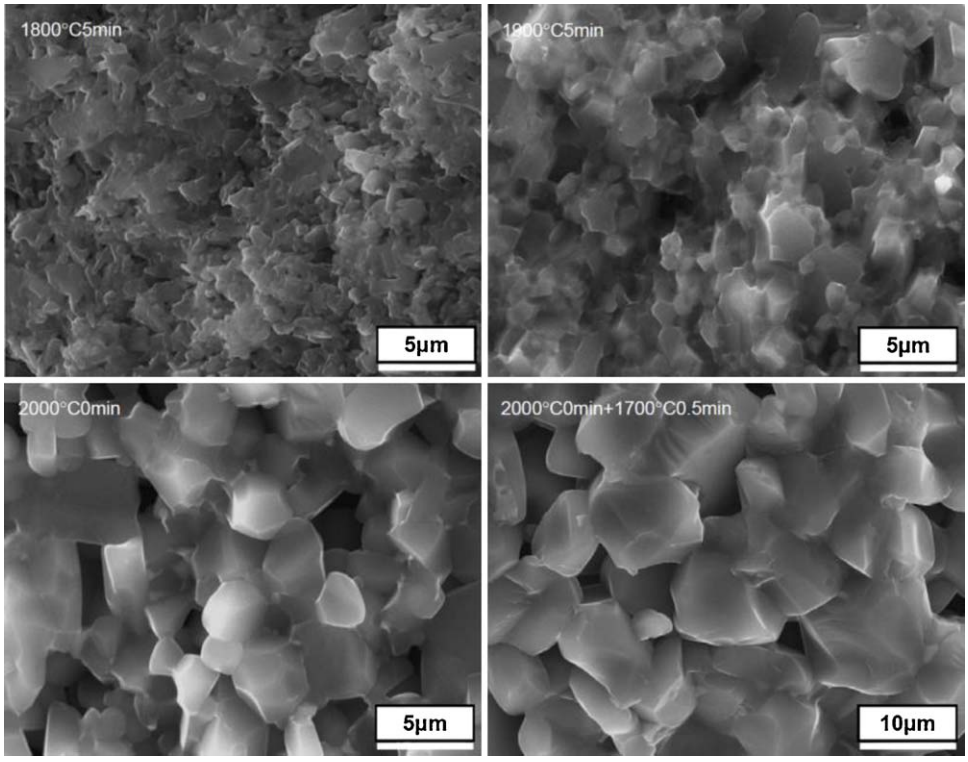


Fig. 4. Fractographs of the materials synthesized under different SPS conditions. Si in the microstructure may weaken the interfacial bonding to give the dominant intergranular fracture mode.

mechanical properties such as flexure strength and creep resistance. We had synthesized the self-toughening α-SiC/α-SiAlON composites with 0–40 wt% 6H SiC by SPS in the previous work [23]. Both the α-SiAlON and the α-SiC grains were elongated and performed significant self-toughening effects. The former success in achieving the self-reinforcement by SPS encouraged us to investigate this composition with a high α-SiC content of 80 wt%.

It seemed the α-SiAlON/α-SiC composites with 80 wt% α-SC addition reached full density by SPS at 1800–2000 °C for 0–5 min. Although the α-SiC grains in the 1800 °C material showed anisotropic growth with high aspect ratio up to 6, the α-SiC grains with an average diameter of 1.2 μm were too thin to perform sufficient reinforcing effects [25]. Therefore, the flexure strength only reached the level for a typical commercial SiC ceramic. Prolonging the holding at 1800 °C seemed to be necessary to achieve a better mechanical performance.

Another factor that required longer holding was the α-SiAlON formation. The ingredients for the α-SiAlON phase in the starting powders were highly isolated by the α-SiC particles. Hold at 1800 °C for 5 min was not enough to form the α-SiAlON phase, as shown by the XRD analysis results in Fig. 2 and Table 2.

Higher sintering temperatures may also worth a try to obtain the ideal microstructure. But sintering at higher temperatures was only practicable under a nitrogen atmosphere higher than 0.6 atm, because $Si_3N_4$ decomposed in the 0.6 atm nitrogen at 1900 °C and above, as shown by the XRD in Fig. 2. Except for $Si_3N_4$ decomposition, 1900 °C seemed more favorable than 1800 °C because the 1900 °C 5 min material had a more significant self-reinforcing microstructure as shown in Fig. 3 and the mechanical properties were higher (Table 2).

However, the optimal sintering temperature should not exceed 1900 °C. 2000 °C was not proper based on the fact that the 2000 °C material showed an equiaxed microstructure. At temperatures higher than 1900 °C, the anisotropic interfacial energies of the different facets which determined the Wulff's configuration of the α-SiC grains seemed diminish, therefore yielded equiaxed α-SiC grains. In Fig. 3 the microstructure of the 2000 °C 0 min material appeared to be equiaxed rather than the elongated growth in the lower temperature materials.

### *4.2. 6H to 3C-SiC phase transformation*

XRD analysis shown in Fig. 2 indicated the 6H SiC completely transformed into the 3C phase in the 2000 °C 0 min + 1700 °C 0.5 min material. Given the slight difference in the sintering conditions between the 2000 °C 0 min + 1700 °C 0.5 min and the 2000 °C 0 min materials, the 6H to 3C-SiC phase transformation actually took place at 1700 °C in the cooling process and completed in the very short time of 30 s.

Transformation of 3C to 6H-SiC (or 4H) was more commonly reported in the literatures than the reverse because the formation of the self-reinforcing microstructures of the SiC ceramics was usually dependent on the 3C to 6H-SiC transformation. An additional advantage by using 3C-SiC rather than using plate-like α-SiC of 4H, 6H, and 15R as the starting powders was that it was much more flexible in microstructure control and easier for densification [6,7,10,11] by using the 3C SiC.

However, the 3C-SiC phase would not grow anisotropic due to the cubic symmetry. Therefore the 6H to 3C-SiC polytype transformation cannot bring a self-toughening microstructure. This can be a part reason why the reports on the 6H to 3C-SiC transformation were very few [26,27].

In spite of the relatively low commercial value of the 3C SiC ceramics, it was very interesting that the 6H to 3C-SiC phase transformation proceeded extremely fast at 1700 °C by passing an electric current through the 6H compact, at presence of the YSiAlON liquid, nitrogen solution and Si melt in the liquid. The 6H to 3C-SiC phase transformation completed in 30 s, in direct comparison with the max 94% transformation by conventional annealing at 2250 °C for 30 min [26].

Incubating at 2000 °C before the 6H to 3C-SiC polytype transformation may have provided some premises for the transformation. SiC nuclei may form after the SiC particles were highly activated by the high temperature. Even if this was the case, however, XRD was ineffective in recognizing 3C SiC nuclei from 6H-SiC due to peak overlapping as shown in Fig. 2. Transmission electron microscopy and selected area electron diffraction are needed and such works are ongoing. Possible mechanisms for the fast 6H to 3C-SiC polytype transformation are also under investigation. The results will be published elsewhere.

As a suspicion, we think the fast 6H to 3C-SiC polytype transformation, at least, was partly correlated with the electric current passing through the SiC compact, for that electric current can enhance material transportation, hence faster solid state phase transformations in metals [28–30]. However, in contrast to the large stack of papers on metals, such study in ceramics is still very limited. The observations reported in this study perhaps are among the first to demonstrate the effects of electric on phase transformation in a common engineering ceramic of SiC.

## 5. Conclusions

α-SiC/α-SiAlON composites with a 20 wt% α-SiAlON addition could be densified by spark plasma sintering in 0–5 min at 1800–2000 °C. The α-SiC grains grew anisotropic by Ostwald ripening in a temperature range of 1800–1900 °C. The small concentrations of $Si_3N_4$, AlN, $Al_2O_3$, and $Y_2O_3$ particles as the α-SiAlON precursors were highly isolated by the 6H-SiC, so that 1800 °C for 5 min was insufficient to diffuse the species to form the desired α-SiAlON phase. At 1900 °C or above temperatures, $Si_3N_4$ decomposed and introduced Si into the phase compositions. The preserved AlN, $Al_2O_3$, $Y_2O_3$ reacted with the $SiO_2$ present on the carbide and nitrides, yielded a large concentration of granular phases in the microstructures. In process of cooling down from 2000 °C, a transitory hold at 1700 °C stimulated 6H → 3C-SiC polytype transformation. The material synthesized at 1900 °C obtained a relatively ideal self-toughening microstructure, hence high flexure strength and fracture toughness.

## Acknowledgements

This work was financially supported by "the Fundamental Research Funds for the Central Universities" under Grant No. HIT. NSRIF 2010111, and China Postdoctoral Science Foundation under Grant No. 20090450957.

## References

1. Rodríguez-Rojas F, Ortiz AL, Borrero-López O, Guiberteau F. Effect of the sintering additive content on the non-protective oxidation behavior of pressureless liquid-phase-sintered α-SiC in air. *J Eur Ceram Soc* 2010;**30**:1513–8.
2. Charpentier L, Balat-Pichelin M, Audubert F. High temperature oxidation of SiC under helium with low-pressure oxygen—Part 1: sintered α-SiC. *J Eur Ceram Soc* 2010;**30**:2653–60.
3. Sánchez-González E, Miranda P, Guiberteau F, Pajares A. Effect of microstructure on the mechanical properties of liquid-phase-sintered silicon carbide at pre-creep temperatures. *J Eur Ceram Soc* 2011;**31**: 1131–9.
4. Rodríguez-Rojas F, Ortiz AL, Guiberteau F, Nygren M. Oxidation behavior of pressureless liquid-phase-sintered α-SiC with additions of $5Al_2O_3 + 3RE_2O_3$ (RE = La, Nd, Y, Er, Tm, or Yb). *J Eur Ceram Soc* 2010;**30**:3209–17.
5. Suzuki TS, Uchikoshi T, Sakka Y. Effect of sintering conditions on microstructure orientation in α-SiC prepared by slip casting in a strong magnetic field. *J Eur Ceram Soc* 2010;**30**:2813–7.
6. Lee SK, Kim CH. Effects of α-SiC versus β-SiC starting powders on microstructure and fracture toughness of SiC sintered with $Al_2O_3$–$Y_2O_3$ additives. *J Am Ceram Soc* 1994;**77**:1655–8.
7. Cao JJ, Moberly Chan WJ, Jonghe L, Gilbert C, Ritchie R. In situ toughened silicon carbide with Al-B-C additions. *J Am Ceram Soc* 1996;**79**: 461–9.
8. Hirata Y, Suzue N, Matsunaga N, Sameshima S. Particle size effect of starting SiC on processing, microstructures and mechanical properties of liquid phase-sintered SiC. *J Eur Ceram Soc* 2010;**30**:1945–54.
9. Neher R, Herrmann M, Brandt K, Jaenicke-Roessler K, Pan Z, Fabrichnaya O, Seifert HJ. Liquid phase formation in the system SiC, $Al_2O_3$, $Y_2O_3$. *J Eur Ceram Soc* 2011;**31**:175–81.
10. Cheong D, Kim J, Kang S. Effects of isothermal annealing on the microstructure and mechanical properties of SiC ceramics hot-pressed with $Y_2O_3$ and $Al_2O_3$ Additions. *J Eur Ceram Soc* 2002;**22**:1321–7.
11. Kovalčíková A, Dusza J, Šajgalík P. Thermal shock resistance an fracture toughening of liquid-phase-sintered SiC-based ceramics. *J Eur Ceram Soc* 2009;**29**:2387–94.
12. Zenotchkine M, Shuba R, Kim JS, Chen I-W. Effect of seeding on the microstructure and mechanical properties of α-SiAlON: I. Y-SiAlON. *J Am Ceram Soc* 2002;**85**:1254–9.
13. Peng H, Shen Z, Nygren M. Formation of in-situ reinforced microstructures in α-SiAlON ceramics: Part III. Static and dynamic ripening. *J Mater Res* 2004;**19**:2402–9.
14. Carman A, Pereloma E, Cheng YB. Reversible α' ↔ β' transformation in a textured Sm-sialon ceramic. *J Eur Ceram Soc* 2011;**31**:1165–75.
15. Acikbas N, Kumar R, Kara F, Mandal H, Basu B. Influence of β-$Si_3N_4$ particle size and heat treatment on microstructural evolution of α:β-SiAlON ceramics. *J Eur Ceram Soc* 2011;**31**:629–35.
16. Kurama S, Schulz I, Herrmann M. Wear properties of α- and α/β-SiAlON ceramics obtained by gas pressure sintering and spark plasma sintering. *J Eur Ceram Soc* 2011;**31**:921–30.
17. Sasaki H, Oumi Y, Sadakane M, Sano T. Synthesis of single phase Ca-α-SiAlON using Y-type zeolite. *J Eur Ceram Soc* 2010;**30**:1537–41.
18. Nordberg LO, Ekström T, Xu FF. Simultaneously $MoSi_2$ and SiC-reinforced α-SiAlON composites. *J Mater Sci Lett* 1997;**16**:917–20.
19. Dong SM, Jiang DL, Tan SH, Guo JK. Hot isostatic pressing and post-hot isostatic pressing of SiC-β-SiAlON composites. *Mater Lett* 1996;**29**:259–63.
20. Santos C, Kelly CA, Ribeiro S, Strecker K, Souza JC, Silva OM. α-SiAlON-SiC composites obtained by gas-pressure sintering and hot-pressing. *J Mater Process Technol* 2007;**189**:138–42.
21. Wang H, Cheng YB, Muddle BC, Gao L, Yen T. Microstructure and mechanical properties of nanoscale SiC/α-SiAlON composites. *J Mater Sci* 1997;**32**:3263–9.
22. Souza JC, Santos C, Kelly CA, Silva OM. Development of α-SiAlON-SiC ceramic composites by liquid phase sintering. *Int J Refract Met Hard Mater* 2007;**25**:77–81.
23. Liu L, Ye F, Zhang Z, Zhou Y. Elongation of α-SiC particles in spark plasma sintered α-SiAlON/α-SiC composites. *J Am Ceram Soc* 2011;**94**: 336–9.
24. Babini GN, Bellosi A, Galassi C. Characterization of hot-pressed silicon nitride-based materials by microhardness measurements. *J Mater Sci* 1987;**22**:1687–93.
25. Becher PF. Microstructural design of toughened ceramics. *J Am Ceram Soc* 1991;**74**:255–69.
26. Jepps NW, Page TF. The 6H-3C "reverse" transformation in silicon carbide compacts. *J Am Ceram Soc* 1981;**12**. C-177–8.
27. Turan S, Knowles KM. α → β reverse phase transformation in silicon carbide in silicon nitride-particulate-reinforced-silicon carbide composites. *J Am Ceram Soc* 1996;**79**:2892–6.
28. Conrad H. Effects of electric current on solid state phase transformations in metals. *Mater Sci Eng A* 2000;**287**:227–37.
29. Mizubayashi H, Kameyama N, Hao T, Tanimoto H. Crystallization under electropulsing suggesting a resonant collective motion of many atoms and modification of thermodynamic parameters in amorphous alloys. *Phys Res B* 2001;**64**(054201):1–10.
30. Kim D, Domenicucci A, Iyer SS. An investigation of electrical current induced phase transformations in the NiPtSi/polysilicon system. *J Appl Phys* 2008;**103**:073708–73711.